The impacts of El Niño on the observed sea ice budget of West Antarctica

James O. Pope[1] [iD]**, Paul R. Holland[1], Andrew Orr[1]** [iD]**, Gareth J. Marshall[1]** [iD]**, and Tony Phillips[1]** [iD]

[1]British Antarctic Survey, Cambridge, UK

Abstract We assess the impact of El Niño-induced wind changes on seasonal West Antarctic sea ice concentrations using reanalysis data and sea ice observations. A novel ice budget analysis reveals that in autumn a previously identified east-west dipole of sea ice concentration anomalies is formed by dynamic and thermodynamic processes in response to El Niño-generated circulation changes. The dipole features decreased (increased) concentration in the Ross Sea (Amundsen and Bellingshausen Seas). Thermodynamic processes and feedback make a substantial contribution to ice anomalies in all seasons. The eastward propagation of this anomaly is partly driven by mean sea ice drift rather than anomalous winds. Our results demonstrate that linkages between sea ice anomalies and atmospheric variability are highly nonlocal in space and time. Therefore, we assert that caution should be applied when interpreting the results of studies that attribute sea ice changes without accounting for such temporally and spatially remote linkages.

1. Introduction

The large decrease in Arctic sea ice concentration over recent decades [e.g., *Stroeve et al.*, 2007] is seen as a clear indicator of climate change and synonymous with recent Arctic temperature amplification [e.g., *Serreze et al.*, 2009]. By contrast, Antarctic sea ice has, until recently, showed a statistically significant increase, at a rate of 1.5% per decade from 1979 to 2013 [*Turner et al.*, 2015]. The current generation of climate models almost all fail to capture this increase, while the decrease in Arctic sea ice is much better reproduced [*Turner et al.*, 2013; *Zunz et al.*, 2013; *Shu et al.*, 2015], suggesting that the models poorly represent the physical process's governing Antarctic sea ice. Moreover, considerable uncertainty still exists as to whether this increase is caused by natural variability or anthropogenic forcings (or some combination), as these factors are known to induce changes to Antarctic sea ice by altering the atmospheric circulation [*Yuan and Martinson*, 2001; *Stammerjohn et al.*, 2008; *Turner et al.*, 2009; *Simpkins et al.*, 2012; *Polvani and Smith*, 2013; *Zunz et al.*, 2013; *Barnes et al.*, 2014; *Li et al.*, 2014; *Ferreira et al.*, 2015; *Meehl et al.*, 2016].

The overall increase in Antarctic sea ice concentration is composed of different regional trends. In West Antarctica there are particularly distinct and opposing trends in the Ross Sea (where sea ice concentration has increased by 5.4% per decade) and the Amundsen and Bellingshausen Seas (where sea ice concentration has reduced by 5.1% per decade) [*Parkinson and Cavalieri*, 2012]. However, these trends do not create a precise dipole; the Ross Sea ice expansion occurs all year round, while Bellingshausen Sea ice loss is primarily summer-intensified [*Holland*, 2014]. Around West Antarctica, the transport of sea ice is dominated by the dynamic response to a climatological quasi-stationary low pressure referred to as the Amundsen Sea Low (ASL) [*Holland and Kwok*, 2012; *Hosking et al.*, 2013; *Meehl et al.*, 2016; *Raphael et al.*, 2016]. This sector is also where robust teleconnections to tropical climate variability occur [*Ding et al.*, 2011; *Schneider et al.*, 2012; *Li et al.*, 2014]. In particular, the El Niño–Southern Oscillation (ENSO) has been strongly linked to changes in sea ice concentration in this region [e.g., *Kwok and Comiso*, 2002; *Stammerjohn et al.*, 2008; *Matear et al.*, 2015; *Kwok et al.*, 2016] and in other regions within the Southern Ocean [*Yuan and Martinson*, 2001; *Holland et al.*, 2005]. During the El Niño phase of ENSO, a Rossby wave train of alternating positive and negative geopotential height anomalies becomes established from the central Pacific to the ASL region, often described as the positive polarity of the Pacific-South American (PSA-1) teleconnection pattern [*Mo and Higgins*, 1998; *Mo and Paegle*, 2001; *Irving and Simmonds*, 2016]. This is associated with a weakening of the ASL [*Marshall and Thompson*, 2016; *Turner*, 2004], resulting in increased sea ice in the Bellingshausen Sea and decreased sea ice in the Ross Sea [*Kwok and Comiso*, 2002; *Dash et al.*, 2013; *Kwok et al.*, 2016]. This tropical teleconnection and its influence on the Antarctic have been found to be enhanced when El Niño coincides with the negative phase of the Southern Annular Mode (SAM) [*Fogt et al.*, 2011, 2012].

Previously, *Holland and Kimura* [2016] calculated an observational sea ice budget to separate the contribution to seasonal changes in sea ice concentration from ice dynamics, thermodynamic melting/freezing, and mechanical ridging. In this paper, a similar approach is used to clarify the effect of El Niño-induced near-surface wind anomalies on West Antarctic sea ice concentration.

2. Materials and Methods

2.1. Data

Monthly ERA-Interim atmospheric reanalysis [*Dee et al.*, 2011] fields of sea level pressure (SLP), 850 hPa temperature, and 10 m wind speed components for the period of 1979 to 2014 were retrieved on a reduced Gaussian N128 latitude/longitude grid, which corresponds to around 0.7° spacing. ERA-Interim was found to be the most reliable reanalysis product over Antarctica by *Bracegirdle and Marshall* [2012], and has been used in recent studies examining the influence of near-surface winds on sea ice [*Holland and Kwok*, 2012; *Holland*, 2014]. The 850 hPa temperature was chosen (instead of surface temperature) to minimize the influence of observed sea ice, which is used as a lower boundary condition within the ERA-Interim reanalysis. Monthly sea ice concentration fields derived from passive microwave brightness temperature (using the Bootstrap2 algorithm) were retrieved on a Southern Hemisphere polar stereographic (25 km × 25 km) grid from 1979 to 2014 [*Comiso*, 2015].

2.2. Sea Ice Budget

Following *Holland and Kimura* [2016], the sea ice budget is presented in terms of the intensification of sea ice, $\partial C/\partial t$, which is the rate of change of sea ice concentration over time [*Holland*, 2014], resulting from changes that are caused by ice dynamics and a residual:

$$\frac{\partial C}{\partial t} = -\nabla.(\boldsymbol{u}C) + f. \tag{1}$$

Here the dynamical contribution to intensification can be assessed according to the ice concentration flux divergence, $\nabla.(\boldsymbol{u}C)$, where C is ice concentration and $\boldsymbol{u}$ is ice velocity. The residual, f, is all intensification not attributable to dynamics. Intensification and flux divergence terms can be derived from observations. In West Antarctica, the residual is dominated by melting and freezing, except in a few regions near the coast where it may represent mass-conserving mechanical processes such as ridging [*Holland and Kimura*, 2016]. The sign convention within the sea ice budget is chosen such that positive terms indicate an increase in sea ice concentration. In this study, the 10 m wind speed components are used as a proxy for ice drift under the assumption that ice is in a state of free drift, at 2% of the absolute speed of the winds and at an angle of 15° to the right of the wind direction. This is a relatively good approximation near the ice edge, where the largest anomalies occur [*Kimura*, 2004]. The wind speed was used as a proxy for ice drift because sea ice drift products are unreliable prior to 1992 [*Holland and Kwok*, 2012], due to temporal inhomogeneities across the different satellites and their sensors [*Haumann et al.*, 2016], and four of our seven chosen El Niño years occurred prior to 1992 (see next section).

2.3. Methodology

Seven El Niño events rated as moderate, strong, or very strong in the Oceanic Niño Index [*NOAA*, 2016] were selected between 1979 and 2014, corresponding to the years 1982/1983, 1986/1987, 1987/1988, 1991/1992, 1997/1998, 2002/2003, and 2009/2010. Monthly anomaly fields of SLP, 10 m wind components, 850 hPa temperatures, sea ice concentration, and sea ice intensification from March through to February were computed by differencing composites of these events from the climatological (1979 to 2014) mean. The statistical significance of the SLP, temperature, and sea ice concentration anomalies was assessed using the Mann-Whitney-Wilcox test [*Pettitt*, 1985]. The use of the test in climate studies is documented in *Pfeifer et al.* [2015].

We apply the budget calculation differently to previous studies. We wish to determine the origin of anomalies in sea ice concentration during El Niño years. Therefore, we decompose the dynamic and thermodynamic contributions to anomalous intensification, $\overline{\frac{\partial \Delta C}{\partial t}}$, where a double overbar denotes a mean over El Niño years.

At leading order, the equation governing such anomalies, derived and described in the supporting information, is

$$\overline{\overline{\frac{\partial \Delta C}{\partial t}}} = -\overline{\overline{\nabla.(\overline{u}\Delta C)}} - \overline{\overline{\nabla.(\Delta u \overline{C})}} + \overline{\overline{\Delta f}} \, . \tag{2}$$

It is important to note that reference to our results has allowed us to represent anomalous ice divergence as the sum of two terms; this approximation may not generally be valid and indeed breaks down in summer within our results. The first term on the right-hand side, $\overline{\nabla.(-u\Delta C)}$, is the ice flux divergence anomaly that results from the mean winds (ice drift), $\overline{u}$, acting upon the anomalous ice concentration, ΔC. Hereafter this is referred to as the dynamic (anomalous concentration) term. The second term on the right-hand side, $\overline{\overline{\nabla.(\Delta u \overline{C})}}$, is the ice flux divergence anomaly that results from anomalous winds, Δu, acting upon the climatological ice concentration $\overline{C}$. This is referred to as the dynamic (anomalous winds) term. The residual anomaly $\overline{\overline{\Delta f}}$ is calculated as the difference between the intensification and the sum of these two dynamic terms, and therefore primarily contains anomalies due to ice thermodynamics. The residual term also contains methodological error due to the ice not being in free drift; any ice divergence that causes intensification but is not reflected in the wind divergence will appear in the residual (see below). Further details on all terms can be found in the supporting information.

3. Results

3.1. Seasonal Climatology

Figure 1a shows that El Niño is associated with a positive SLP anomaly of around 3 hPa in the Amundsen Sea region in autumn, consistent with a weakening of the ASL. This anomaly strengthens to around 6 hPa and shifts eastward during winter and spring, such that it is located over the Bellingshausen Sea during spring (Figures 1b and 1c), in agreement with earlier studies [*Kwok and Comiso*, 2002; *Fogt et al.*, 2011, 2012; *Kwok et al.*, 2016]. In summer (Figure 1d), the anomaly weakens and becomes more diffuse (actually expanding to encompass much of Antarctica). The progression of the SLP anomaly through the seasons is controlled by the relationship between the SAM and El Niño [*Fogt et al.*, 2012]. Figures 1e–1g show that El Niño is also associated with a statistically significant east-west dipole pattern of anomalous 850 hPa temperatures up to 2.5°C, with warming in the Ross Sea and cooling in the Amundsen and Bellingshausen Seas. Similarly, an east-west dipole pattern of anomalous sea ice concentration (Figures 1i–1k) of up to 30% occurs, with decreased concentration in the Ross Sea and increased concentration in the Amundsen and Bellingshausen Seas. Both temperature and sea ice concentration dipole anomalies shift eastward during winter and spring, such that during the latter season the region of increased temperature and decreased concentration is found over the Amundsen Sea and the region of decreased temperature and increased concentration is solely over the Bellingshausen Sea. In summer, the anomalous temperature and sea ice concentration conditions become much less coherent and lose the dipole-like pattern, consistent with changes in SLP (cf. Figures 1h and 1l). The breakdown of the dipole structures in the summer is consistent with the relationship between El Niño and the SAM [*Fogt et al.*, 2011, 2012].

The seasonal eastward progression of the sea ice concentration anomaly could occur in response to the shifting anomaly in the winds or be caused by the mean ice drift, which is strongly eastward in this region [*Kimura*, 2004]. We note that the anomalies move eastward at a rate of approximately 15 cm s^{-1} (Figure 2), consistent with the observed rates of sea ice drift for this region [*Kimura*, 2004]. Therefore, to isolate which processes are causing the seasonal ice anomalies, it is necessary to analyze the associated anomalies in the sea ice budget (Figure 3).

3.2. Sea Ice Budget: Dynamic Formation of the Sea Ice Anomaly

In autumn, a positive sea ice intensification anomaly in the Bellingshausen Sea (Figure 3a) indicates that more sea ice is being produced here in this season during El Niño conditions. This is responsible for a strengthening of the positive sea ice concentration anomaly in the Bellingshausen Sea in winter compared to autumn (Figures 1i and 1j). We note that in autumn, the pattern of sea ice intensification anomalies (Figure 3a) resembles the contribution from the dynamic (anomalous winds) term (Figure 3e), suggesting that they are being driven by sea ice transport resulting from the anomalous El Niño circulation. There is a significant residual remaining (Figure 3m), with a structure similar to the intensification anomaly and dynamic (anomalous winds) terms (Figures 3a and 3e). The residual anomaly shows increased intensification in the
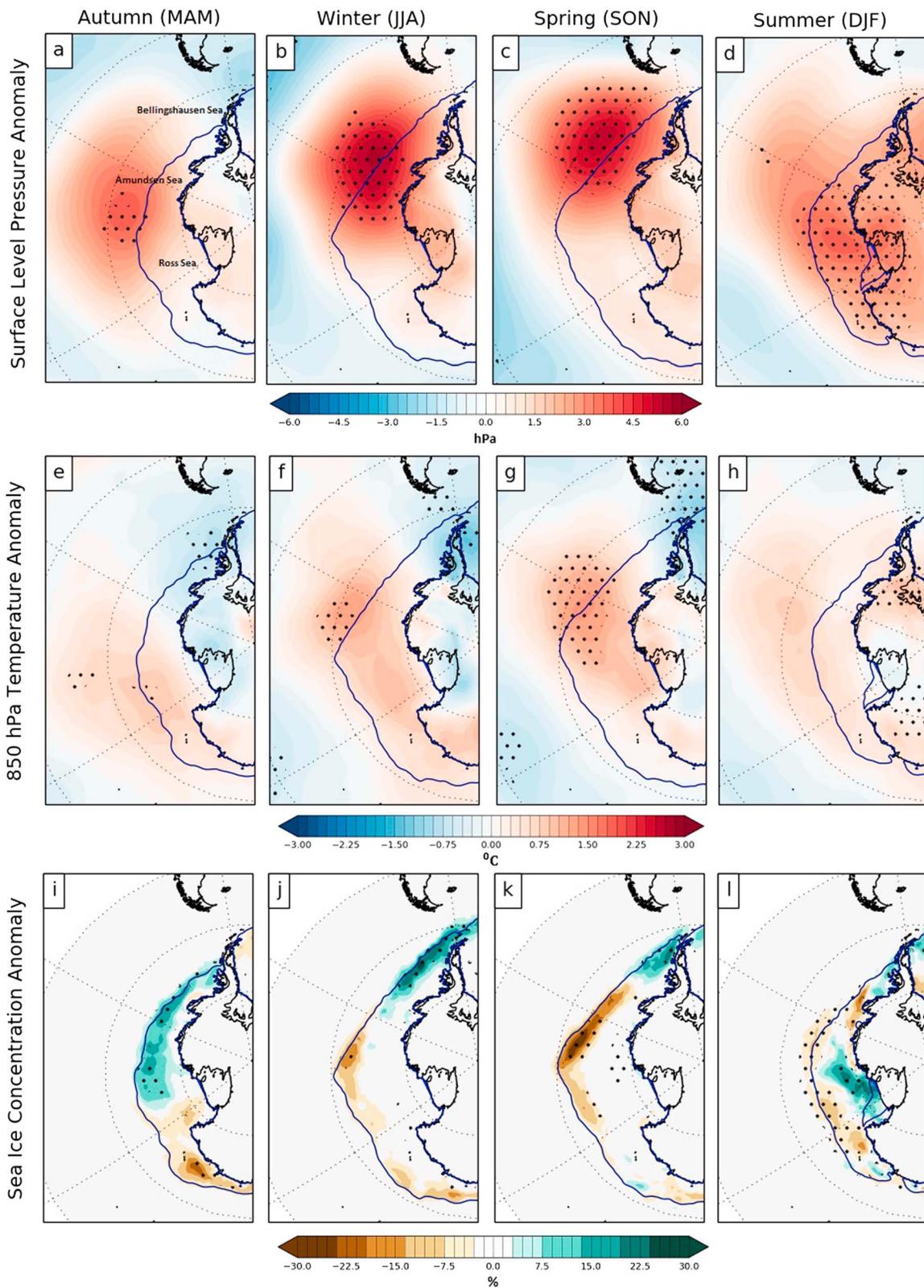
Figure 1. (a–d) Seasonal sea level pressure (units of hPa), (e–h) 850 hPa temperature (units of °C), and (i–l) sea ice concentration (in units of percent) anomalies due to El Niño. The blue line indicates the climatological mean seasonal sea ice extent, defined as the limit of 15% concentration. Stippling indicates significance at 95% confidence for sea level pressure and temperature and 90% for sea ice concentration. The locations of the Ross, Amundsen, and Bellingshausen Seas are indicated in Figure 1a.
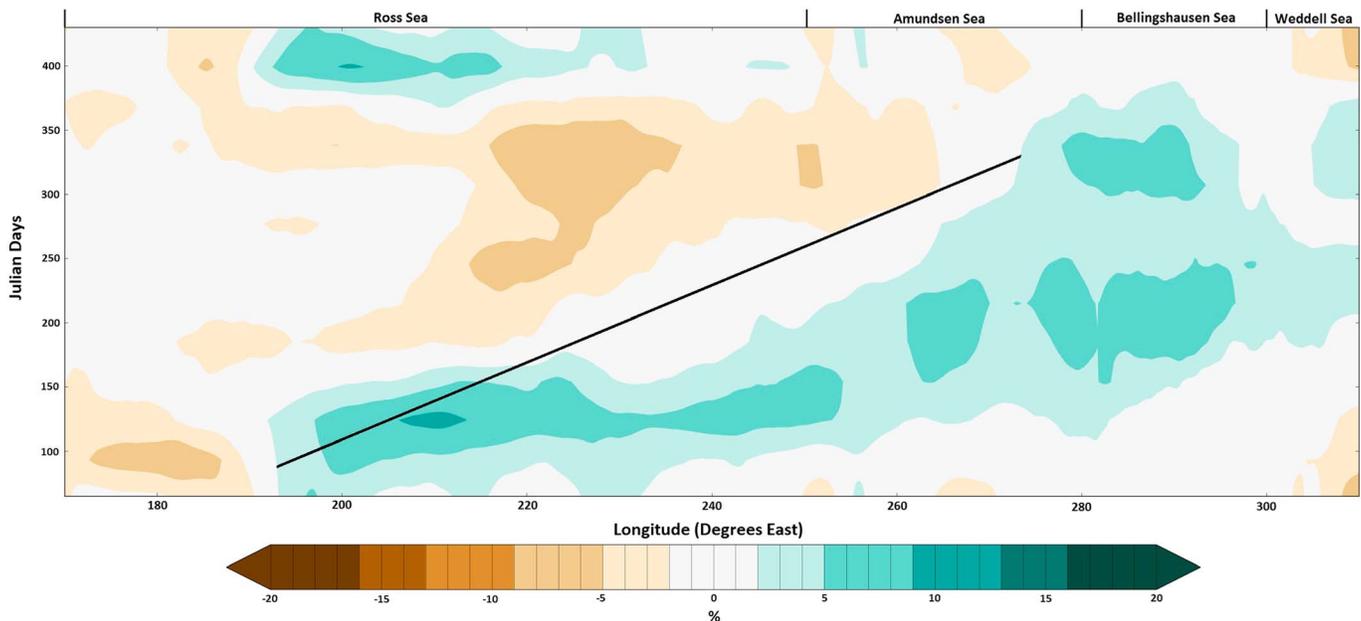
Figure 2. A Hovmöller diagram showing the changes in sea ice concentration anomalies due to El Niño from Bootstrap2 data as a function of time and longitude. The anomaly is averaged over the latitudes 60°S to 75°S. The ice drift speed was calculated based on the seasonal progression of the positive anomaly which was calculated between 195° and 275° over the course of 230 days, denoted by the solid black line. The final value was calculated based on using a value of 38,186 m per degree of longitude.

Bellingshausen Sea and broadly decreased intensification over the Amundsen and eastern Ross Seas, which we interpret as changes in freezing directly induced by anomalies in atmospheric temperature, humidity, and other variables (Figure 1e).

3.3. Sea Ice Budget: Development and Propagation of the Sea Ice Anomaly

In winter, a negative intensification anomaly in the Amundsen and Bellingshausen Seas (Figure 3b) shows that in contrast to autumn, less sea ice is being produced here under El Niño conditions. This results in an enhancement of the negative sea ice concentration anomaly in the Amundsen Sea and a weakening in the anomaly in the Bellingshausen Sea in spring compared to winter (Figures 1j and 1k). However, the dynamic (anomalous winds) term continues to produce a largely similar pattern during winter and spring, with only a slight eastward drift corresponding to changes in the SLP anomaly (Figures 3f and 3g). Therefore, it cannot be responsible for the intensification anomalies during winter and spring (Figures 3b and 3c). This result is unsurprising because the dynamic (anomalous winds) term is only one part of the ice anomaly induced by El Niño. The dynamic (anomalous concentration) term accounts for advection of anomalous ice concentration by the mean winds (see section 2.3), in addition to the residual term representing thermodynamic and mechanical processes.

During winter, residual processes dominate (Figure 3n), and we interpret this as reflecting the role of thermodynamic feedback acting upon anomalies formed during autumn. For example, if ice appears in autumn it cannot appear in winter, so an early ice advance at any given location is represented in our budget as a positive intensification anomaly in autumn and a negative anomaly in winter. In the Bellingshausen Sea, for example, El Niño years have low intensification closer to the coast during winter (Figure 3b) because the ice there formed anomalously early, in autumn (Figure 3a). This is manifested through reduced thermodynamic growth, hence a negative residual anomaly (Figure 3n). However, a positive residual intensification anomaly occurs offshore of this (north of the climatological mean extent line), which we attribute to directly enhanced freezing because the air temperature anomaly is still present (Figure 1f). The opposite pattern occurs in the Ross and Amundsen Seas; late ice advance means there is more winter intensification within the ice pack, and a persistent warm anomaly causes less winter intensification offshore.

In spring the overall intensification (Figure 3c) closely resembles the residual (Figure 3o). The ice is melting, and faster melting corresponds to a negative intensification anomaly. The residual anomalies at the ice
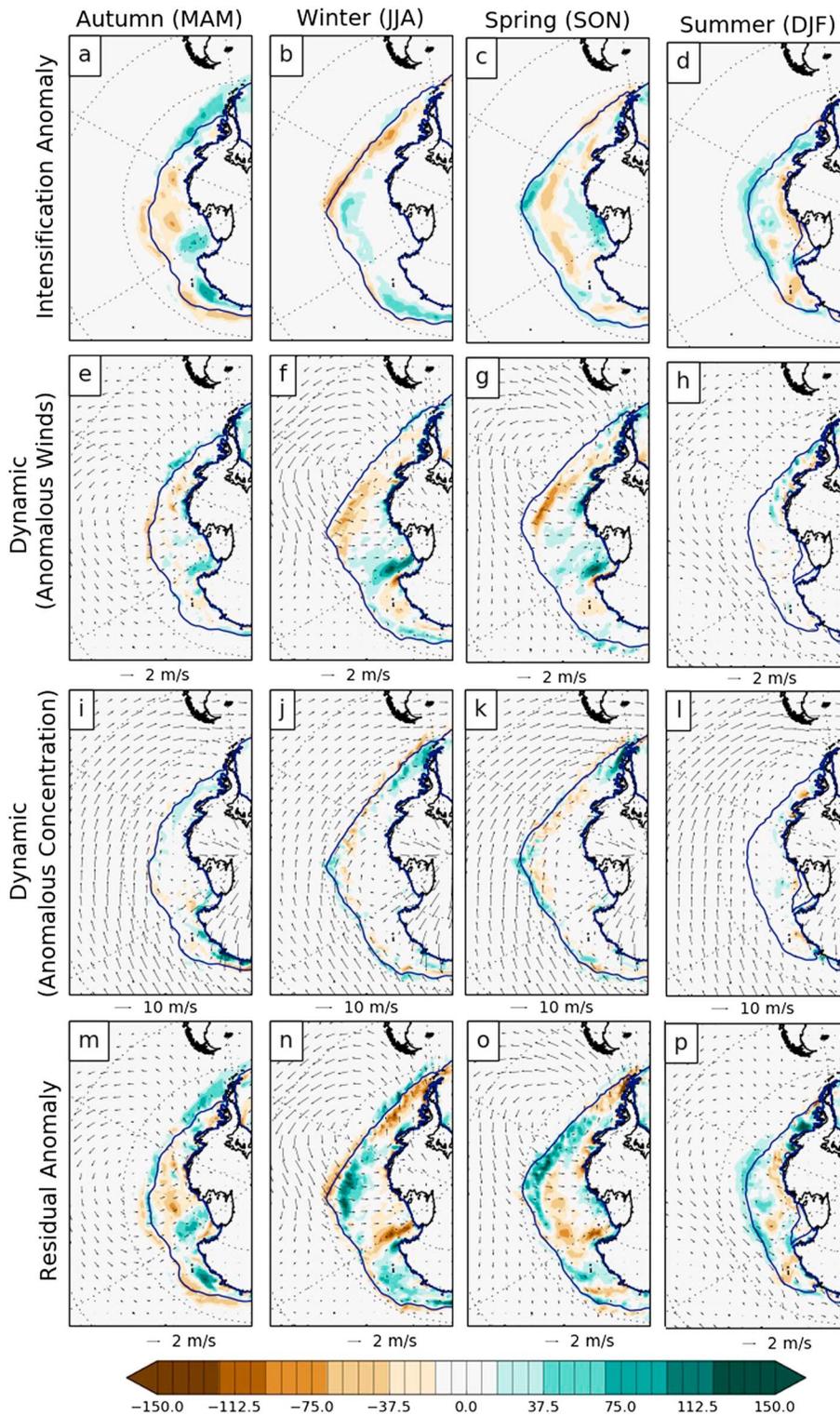
Figure 3. Predicted anomalies in the sea ice budget in El Niño years, using surface winds as a proxy for anomalous ice drift. (a–d) The seasonal intensification anomaly means, $\overline{\frac{\partial \Delta C}{\partial t}}$. (e–h) The seasonal dynamic forcing due to anomalous winds acting upon climatological ice concentration, $-\overline{\nabla.\left(\Delta u \overline{C}\right)}$; vectors show anomalous winds. (i–l) The seasonal dynamic forcing due to climatological winds acting upon anomalous ice concentration, $-\overline{\nabla.\left(\overline{u}\Delta C\right)}$; vectors show climatological winds. (m–p) The residual anomaly ($\overline{\Delta f}$), the difference between the intensification (Figures 3a–3d) and the sum of the two dynamic components (Figures 3e–3h and Figures 3i–3l). The vectors show anomalous winds, as also displayed in the second row. Section 2.3 and the supporting information provide a full description of these terms.

edge have the opposite sign to those that would be expected from the anomalous winds, and so these changes must result from thermodynamic feedback, rather than direct forcing. An early ice retreat appears as a negative intensification anomaly in winter and a positive anomaly in spring (the ice cannot disappear in spring because it has already disappeared in winter). The spring intensification field in the Ross and Amundsen Seas shows positive anomalies at the ice edge, because the ice retreated previously or never grew (Figure 3o). Negative anomalies occur inshore because the ice that does exist in these seasons is still being melted at an anomalously high rate, caused either by feedback (e.g., thin ice melts faster) or the ongoing atmospheric temperature anomalies (Figure 1g).

Additionally, during spring, the ice drift, represented by the dynamic (anomalous concentration) term (Figure 3k), also clearly resembles the intensification anomalies at the sea ice edge (Figure 3c), demonstrating that the advection of anomalies formed in earlier seasons is not negligible. The changing role of the dynamic contributions to ice anomalies is also visible in Figure 2. During autumn and winter (days 60 to 240), the positive sea ice concentration anomaly propagates more slowly than the mean ice drift, consistent with direct forcing from the moving SLP anomaly. However, during spring (days 240 to 310), the eastward propagation accelerates to the mean ice speed, highlighting the importance of ice dynamic anomalies to the development of the ice concentration anomalies.

In summer, the pattern and size of intensification anomalies are inconsistent with the negligible contribution from both dynamic terms (Figures 3h and 3l) and are thus dominated by residual processes (Figure 3p). This is unsurprising because the mean ice budget is dominated by thermodynamics in summer [*Holland and Kimura*, 2016].

3.4. Sea Ice Budget: Remaining Residual Effects

In addition to the residual components caused by direct thermodynamic forcing and thermodynamic feedback, discussed above, there are two remaining sources that contribute to the residual in all seasons. We interpret these as (1) mechanical processes and (2) methodological error due to ice not being in a state of free drift. Features near the coast cannot be simply attributed to thermodynamics because the budget residual is very complex in these regions. First, ice mechanical contributions become important [*Holland and Kimura*, 2016]. When the ice is compressed against the coast, ice concentration can remain constant (e.g., at 100%) because dynamic convergence causes thickening rather than intensification; the implied ice sink can then be incorrectly interpreted as melting in the budget. Second, near the coast the ice is not drifting freely, so the wind anomaly becomes a very poor approximation to the ice drift anomaly [*Kimura*, 2004]. Therefore, we do not attempt to interpret the residual in these regions. The relationship between potentially questionable ice dynamic anomalies and the residual is particularly apparent in the south west Ross Sea embayment during winter and spring.

4. Conclusions

Using the ERA-Interim reanalysis from 1979 to 2014, we created a composite of seven El Niño events. During autumn, winter, and spring a statistically significant positive SLP anomaly occurs off West Antarctica, indicating a reduction in the depth of the ASL. In summer, a SLP anomaly is established across most of Antarctica. These changes are the result of the El Niño tropical sea surface temperature forcing acting on the ASL via the positive polarity of the PSA-1 teleconnection. Contemporaneously, sea ice concentration anomalies were computed, and an east-west concentration dipole observed during autumn, winter, and spring. In autumn, the region of decreased concentration is located in the Ross Sea with increased concentration in the Amundsen and Bellingshausen Seas. The sea ice concentration dipole subsequently progresses eastward in line with the SLP anomaly through winter and spring, such that during spring the negative anomaly is located in the Amundsen Sea and the positive anomaly in the Bellingshausen Sea. The seasonal progression of this anomaly is consistent with the mean rate of sea ice drift.

To determine the role of the changes in Antarctic near-surface circulation due to El Niño on these ice concentration anomalies, we used surface wind anomalies as a proxy for ice drift, and then considered the resultant sea ice budget. In autumn, El Niño-driven sea ice intensification is instigated by dynamic and thermodynamic processes due to anomalous wind forcing and atmospheric temperature changes. During winter, residual processes, principally thermodynamic feedback resulting from the dynamically driven autumn anomalies,

dominate the sea ice budget. In the spring, the concentration dipole that formed in autumn is advected eastward with the mean ice drift. This interpretation is consistent with observed drift speeds at the ice edge, indicating that while wind forcing initiates the ice anomaly, thereafter it is influenced by the average drift of sea ice. Strong thermodynamic feedback also occur in spring, with freezing and melting significantly affected by anomalous ice advance and retreat in previous seasons. Thermodynamic anomalies are dominant during the summer.

The results of this study help determine the processes through which natural variability (in this case El Niño events) plays a role in driving regional Antarctic sea ice changes. To our knowledge, our anomaly sea ice budget approach has for the first time allowed us to quantify the importance of thermodynamic feedback and ice anomaly advection by mean ice drift. Almost all previous studies have considered ice-climate linkages to be static in either space or time, or both. For example, using our approach, it becomes clear that the ice anomaly in the Bellingshausen Sea in spring is affected by anomalous winds and air temperature in the Ross Sea in autumn. Interseasonal thermodynamic feedback are also apparent in all regions. These considerations underline the complexity of climate processes and suggest that caution must be employed when interpreting the results of the many studies that link sea ice extent in any given region or season to local forcings [e.g., *Holland and Kwok*, 2012; *Holland*, 2014; *Li et al.*, 2014; *Kwok et al.*, 2016; *Meehl et al.*, 2016].

References

Barnes, E. A., N. W. Barnes, and L. M. Polvani (2014), Delayed southern hemisphere climate change induced by stratospheric ozone recovery, as projected by the CMIP5 models, *J. Clim.*, *27*, 852–867, doi:10.1175/JCLI-D-13-00246.1.

Bracegirdle, T. J., and G. J. Marshall (2012), The reliability of Antarctic tropospheric pressure and temperature in the latest global reanalyses, *J. Clim.*, *25*, 7138–7146, doi:10.1175/JCLID-11-00685.1.

Comiso, J. (2015), Bootstrap sea ice concentrations from Nimbus-7 SMMR and DMSP SSM/I-SSMIS, Version 2., NASA Natl. Snow and Ice Data Cent. Distributed Active Archive Centers.

Dash, M. K., P. C. Pandey, N. K. Vyas, and J. Turner (2013), Variability in the ENSO-induced southern hemispheric circulation and Antarctic sea ice extent, *Int. J. Climatol.*, *33*, 778–783, doi:10.1002/joc.3456.

Dee, D. P., et al. (2011), The ERA-Interim reanalysis: Configuration and performance of the data assimilation system, *Q. J. R. Meteorol. Soc.*, *137*, 553–597, doi:10.1002/qj.828.

Ding, Q., E. J. Steig, D. S. Battisti, and M. Küttel (2011), Winter warming in West Antarctica caused by central tropical Pacific warming, *Nat. Geosci.*, *4*, 398–403, doi:10.1038/NGEO1129.

Ferreira, D., J. Marshall, C. M. Bitz, S. Solomon, and R. A. Plumb (2015), Antarctic ocean and sea ice response to ozone depletion: A two time scale problem, *J. Clim.*, *25*, 6646–6665, doi:10.1175/JCLI-D-14-00313.1.

Fogt, R. L., D. H. Bromwich, and K. M. Hines (2011), Understanding the SAM influence on the South Pacific ENSO teleconnection, *Clim. Dyn.*, *36*, 1555, doi:10.1007/s00382-010-0905-0.

Fogt, R. L., J. M. Jones, and J. Renwick (2012), Seasonal zonal asymmetries in the Southern Annular Mode and their impact on regional temperature anomalies, *J Clim.*, *25*, 6253–6270, doi:10.1175/JCLI-D-11-00474.1.

Haumann, F. A., N. Gruber, M. Münnich, I. Frenger, and S. Kern (2016), Sea-ice transport driving Southern Ocean salinity and its recent trends, *Nature*, *537*, 89–92, doi:10.1038/nature19101M3.

Holland, M. M., C. M. Bitz, and E. C. Hunke (2005), Mechanisms forcing an Antarctic dipole in simulated sea ice and surface ocean conditions, *J. Clim.*, *18*, 2052–2066, doi:10.1175/JCLI3396.1.

Holland, P. R. (2014), The seasonality of Antarctic sea ice trends, *Geophys. Res. Lett.*, *41*, 4230–4237, doi:10.1002/2014GL060172.

Holland, P. R., and R. Kwok (2012), Wind-driven trends in Antarctic sea-ice drift, *Nat. Geosci.*, *5*, 872–875, doi:10.1038/ngeo1627.

Holland, P. R., and N. Kimura (2016), Observed concentration budgets of Arctic and Antarctic sea ice, *J. Clim.*, *29*, 5241–5249, doi:10.1175/JCLI-D-16-0121.1.

Hosking, J. S., A. Orr, G. J. Marshall, J. Turner, and T. Phillips (2013), The influence of the Amundsen-Bellingshausen Sea low on the climate of West Antarctica and its representation in coupled climate model simulations, *J. Clim.*, *26*, 6633–6648, doi:10.1175/JCLI-D-12-00813.1.

Irving, D., and I. Simmonds (2016), A new method for identifying the Pacific-South American pattern and its influence on regional climate variability, *J. Clim.*, *29*, 6109–6125, doi:10.1175/JCLI-D-15-0843.1.

Kimura, N. (2004), Sea ice motion in response to surface wind and ocean current in the Southern Ocean, *J. Meteorol. Soc. Japan*, *82*, 1223–1231, doi:10.2151/jmsj.2004.1223.

Kwok, R., and J. C. Comiso (2002), Spatial patterns of variability in Antarctic surface temperature: Connections to the Southern Hemisphere Annular Mode and the Southern Oscillation, *Geophys. Res. Lett.*, *29*(14), 1705, doi:10.1029/2002GL015415.

Kwok, R., J. C. Comiso, T. Lee, and P. R. Holland (2016), Linked trends in sea ice edge and Southern Oscillation Index in the Pacific sector of the Southern Ocean: 1982–2013, *Geophys. Res. Lett.*, *43*, 10,295–10,302, doi:10.1002/2016GL070655.

Li, X., D. M. Holland, E. P. Gerber, and Y. Changhyun (2014), Impacts of the north and tropical Atlantic Ocean on the Antarctic Peninsula and sea ice, *Nature*, *505*, 538–542, doi:10.1038/nature12945.

Marshall, G. J., and D. W. J. Thompson (2016), The signatures of large-scale patterns of atmospheric variability in Antarctic surface temperatures, *J. Geophys. Res. Atmos.*, *121*, 3276–3289, doi:10.1002/2015JD024665.

Matear, R. J., T. J. O'Kane, J. S. Risbey, and M. Chamberlain (2015), Sources of heterogeneous variability and trends in Antarctic sea-ice, *Nat. Commun.*, *6*, 8656, doi:10.1038/ncomms9656.

Meehl, G. A., J. M. Arblaster, C. M. Blitz, C. T. Y. Chung, and H. Teng (2016), Antarctic sea-ice expansion between 2000 and 2014 driven by tropical Pacific decadal climate variability, *Nat. Geosci.*, *9*, 590–595, doi:10.1038/ngeo2751.

Mo, K. C., and R. W. Higgins (1998), The Pacific-South American modes and tropical convection during the southern hemisphere winter, *Mon. Weather Rev.*, *126*, 1581–1596, doi:10.1175/1520-0493(1998)126<1581:TPSAMA>2.0.CO;2.

Mo, K. C., and J. N. Paegle (2001), The Pacific-South American modes and their downstream effects, *Int. J. Climatol.*, *21*, 1211–1229, doi:10.1002/joc.685.

NOAA (2016), Oceanic Niño index. NOAA National Weather Service, Center for Climate Prediction. [Available at http://www.cpc.ncep.noaa.gov/products/analysis_monitoring/ensostuff/ensoyears.shtml.]

Parkinson, C. L., and D. J. Cavalieri (2012), Antarctic sea ice variability and trends, 1979–2010, *Cryosphere*, *6*, 871–880, doi:10.5194/tc-6-871-2012.

Pettitt, A. (1985), Mann-Whitney-Wilcoxon statistic, in *Encyclopedia of Statistical Sciences*, vol. 5, edited by S. Kotz, N. L. Johnson, and C. B. Read, pp. 208–211, Wiley, New York.

Pfeifer, S., K. Bülow, A. Gobiet, A. Hänsler, M. Mudelsee, J. Otto, D. Rechid, C. Teichmann, and D. Jacob (2015), Robustness of ensemble climate projections analyzed with climate signal maps: Seasonal and extreme precipitation for Germany, *Atmosphere*, *6*, 677–698, doi:10.3390/atmos6050677.

Polvani, L. M., and K. L. Smith (2013), Can natural variability explain observed Antarctic sea ice trends? New modeling evidence from CMIP5, *Geophys. Res. Lett.*, *40*, 3195–3199, doi:10.1002/grl.50578.

Raphael, M. M., G. J. Marshall, J. Turner, R. L. Fogt, D. Schneider, D. A. Dixon, J. S. Hosking, J. M. Jones, and W. R. Hobbs (2016), The Amundsen Sea low: Variability, change and impact on Antarctic climate, *Bull. Am. Meteorol. Soc.*, *8*, 111–121, doi:10.1175/BAMD-D-14-00018.1.

Schneider, D. P., Y. Okumura, and C. Deser (2012), Observed Antarctic interannual climate variability and tropical linkages, *J. Clim.*, *25*, 4048–4066, doi:10.1175/JCLI-D-11-00273.1.

Serreze, M. C., A. P. Barrett, J. C. Stroeve, D. N. Kindig, and M. M. Holland (2009), The emergence of surface-based Arctic amplification, *Cryosphere*, *3*, 11–19, doi:10.5194/tc-3-11-2009.

Shu, Q., Z. Song, and F. Qiao (2015), Assessment of sea ice simulations in the CMIP5 models, *Cryosphere*, *9*, 399–409, doi:10.5194/tc-9-399-2015.

Simpkins, G. R., L. M. Ciasto, D. W. J. Thompson, and M. H. England (2012), Seasonal relationships between large-scale climate variability and Antarctic sea ice concentration, *J. Clim.*, *25*, 5451–5469, doi:10.1175/JCLI-D-11-00367.1.

Stammerjohn, S. E., D. G. Martinson, R. C. Smith, X. Yuan, and D. Rind (2008), Trends in Antarctic annual sea ice retreat and advance and their relation to El Niño–southern Oscillation and Southern Annular Mode variability, *J. Geophys. Res.*, *113*, C03S90, doi:10.1029/2007JC004269.

Stroeve, J., M. M. Holland, W. Meier, T. Scambos, and M. Serreze (2007), Arctic sea ice decline: Faster than forecast, *Geophys. Res. Lett.*, *34*, L09501, doi:10.1029/2007GL029703.

Turner, J. (2004), The El-Niño-Southern Oscillation and Antarctica, *Int. J. Climatol.*, *24*, 1–31, doi:10.1002/joc.965.

Turner, J., J. C. Comiso, G. J. Marshall, T. A. Lachlan-Cope, T. Bracegirdle, T. Maksym, M. P. Meredith, Z. Wang, and A. Orr (2009), Non-annular atmospheric circulation change induced by stratospheric ozone depletion and its role in the recent increase of Antarctic sea ice extent, *Geophys. Res. Lett.*, *36*, L08502, doi:10.1029/2009GL037524.

Turner, J., T. J. Bracegirdle, T. Phillips, G. J. Marshall, and J. S. Hosking (2013), An initial assessment of Antarctic sea ice extent in the CMIP5 models, *J. Clim.*, *26*, 1473–1484, doi:10.1175/JCLI-D-12-00068.1.

Turner, J., J. S. Hosking, T. J. Bracegirdle, G. J. Marshall, and T. Phillips (2015), Recent changes in Antarctic sea ice, *Philos. Trans. R. Soc., A.*, *373*, 20140163, doi:10.1098/rsta.2014.0163.

Yuan, X., and D. G. Martinson (2001), The Antarctic dipole and its predictability, *Geophys. Res. Lett.*, *28*, 3609–3612, doi:10.1029/2001GL012969.

Zunz, V., H. Goosse, and F. Massonnet (2013), How does internal variability influence the ability of CMIP5 models to reproduce the recent trend in Southern Ocean sea ice extent?, *Cryosphere*, *7*, 451–468, doi:10.5194/tc-7-451-2013.